NRIAG Journal of Astronomy and Geophysics (2014) 3, 150–162

National Research Institute of Astronomy and Geophysics

NRIAG Journal of Astronomy and Geophysics

www.elsevier.com/locate/nrjag

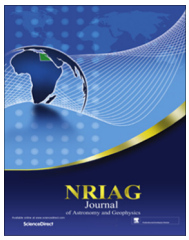

# Geotechnical studies for evaluation and limitations of environmental and engineering hazards that affect the economic infrastructure in Abha, Saudi Arabia

**Fathy Shaaban** [a,b,*], **Ali E. Al-Salami** [a]

[a] *Physics Department, Faculty of Science, King Khaled University, Saudi Arabia*
[b] *National Research Institute of Astronomy and Geophysics, Egypt*

Received 8 April 2013; revised 14 August 2014; accepted 10 October 2014
Available online 2 December 2014

**KEYWORDS**

Geotechnical;
Environmental;
Hazards;
Infrastructure and Abha

**Abstract** Abha is the capital of Asir province in Saudi Arabia. It is situated 2200 meters (7200 ft) above the sea level in the fertile mountains of the south-western Saudi Arabia. One of the most important structures of this region is Abha dam that acts as a barrier that impounds water or underground streams thereby retaining the ground water of the region. With the passage of time, various environmental factors such as ground movement, wind and changes in temperature may have significant effect on these various structure factors and may lead to invisible cracks and other structural defects. Because the dams and tunnels are prone to sudden collapse, there is potential great risk to lives of the people and significant economic loss in this area. The use of the ground penetrating radar (GPR) and electric resistivity techniques is a non-invasive scan and could assess the conditions of various built structures as well as the earth beneath or surrounding it. So the GPR system with appropriate types of antennas (1.5 GH, 1 GH, 400 MH and 100 MH) and electrical resistivity in one dimension (VES) and two dimensions (electrical profiling and imaging) is used in this work. This work aims to investigate the dam structure, developing cracks or areas of increased moisture. Also to study the surrounding areas to detect seepage from pond that may affect nearby buildings and the dam itself.

It reveals that, the depth of water bearing layer ranges from 2 m to 10 m, where the three geoelectric layers are present. The first layer has resistivity values ranging from 44 Ω m–1200 Ω m with thickness ranging from 3 m to 18 m that is interpreted as the wadi deposits. The second layer having resistivity values from 11 Ω m to 137 Ω m is interpreted as the water saturated in the fractured basements. The

* Corresponding author at: Physics Department, Faculty of Science, King Khaled University, Saudi Arabia.
E-mail address: shaaban_F@hotmail.com (F. Shaaban).

Peer review under responsibility of National Research Institute of Astronomy and Geophysics.

ELSEVIER Production and hosting by Elsevier

http://dx.doi.org/10.1016/j.nrjag.2014.10.002

third layer of resistivity values ranging from 2200 Ω m to 90,000 Ω m is interpreted as dry, massive basements. The GPR results provided internal images of the slab, showing its morphology, areas of possible damage and changes to the structure, and the situation of the steel reinforcements. It showed the presence of different shapes of fractures and voids with the growing of moisture zones.



## 1. Introduction

Increased public awareness of pollution in the environment in both the industrial and military sectors as well as geotechnical and engineering problems have encouraged a continuing search for innovative and cost-effective means for understanding near-surface structure. More and more contractors and government agencies over the past few years have recognized the benefits and cost savings of using geophysical methods in conducting their geotechnical investigations. Newer and more capable instruments combined with faster computers have enabled the widespread use of various methods for locating and identifying subsurface features and structures that will impact construction designs.

Applied geophysics investigates the physical properties of the ground, providing vital information on subsurface material conditions for numerous practical applications. Geophysical investigations are non-invasive and avoid the disruption caused by invasive testing such as drilling and pitting. In environments where invasive investigations are not permissible, geophysics can provide detailed information on subsurface structures and help answer questions for successful construction and infrastructure maintenance of large areas. The Physics Department of King Khaled University provides geophysical services for civil engineering, environmental science, archeology and non-destructive testing applications.

Abha is the capital of Asir province in Saudi Arabia. It is situated 2200 meters (7200 ft) above sea level in the fertile mountains of the south-western Saudi Arabia. One of the most important structures in this region is Abha dam (Fig. 1), that acts as a barrier that impounds water or underground streams there by retaining the ground water of the region.

With time, various environmental factors such as ground movement, wind and changes in temperature may have significant effect on these various structure factors. These factors may lead to cracks and other structural defects may be invisible. Because the dams, tunnels are prone to sudden collapse, there is potential great risk for the people and economy (Tsoflias et al., 2004).

One of these cost-effective methods for non-invasive sub surface scanning is the ground penetrating radar (GPR) technique. This technique is used successfully in the detection of cracks, voids and other anomalies appearing with the aging of such materials. GPR is a pulse echo method for measuring pavement layer thickness' and properties. GPR uses electromagnetic waves to penetrate the pavement by transmitting the wave energy into the pavement from a moving antenna. These waves travel through the pavement structure and echoes are created at boundaries of dissimilar materials. The arrival and strength of these echoes can then be used to calculate pavement layer thickness and other properties like moisture content. It is therefore necessary to do a geotechnical survey to determine the extent of the stability of these components of the infrastructure (Davis and Annan, 1989; Davis et al., 1984).

An evaluation of the physical condition of concrete is crucial for predicting the life of reinforced concrete structures. For example, it is well known that water and chloride contents are among the concrete features that govern reinforcing bar corrosion (Andrade et al., 1999; Raupach, 1996). It is then necessary to assess the spatial distribution of these physical features throughout the structure to improve the pathology diagnosis. However, the on-site evaluation of these durability indicators is difficult and often requires destructive tests (Matthews et al., 1998).

Among the various non-destructive evaluation techniques, radar has become an interesting instrument for the rapid evaluation of reinforced concrete structures regarding the detection and location of buried objects such as steel rebar. In addition, radar waves propagating through concrete are affected by changes in the moisture content. For example, several authors have reported that radar wave velocity is reduced when the concrete moisture increases (Laurens, 2001; Klysz et al., 2004; Sbartaï, 2005). Recently, Sbartaï et al. (2006a) showed that an increase in the chloride content of concrete leads to a significant decrease in the amplitude of both direct and reflected waves. In addition Sbartaï (2005) also showed that the velocity of radar waves is mainly affected by moisture variations. For dry and wet concrete, water/concrete ratio did not appear as an influent parameter on radar signals variation (Sbartaï et al., 2006b).

Results are presented in an easy way to understand engineering compatible CAD format. A typical ground radar system comprises an antenna unit, control console, display monitor and graphic printer. The antenna unit is in direct ground contact, with the remaining equipment either vehicle-mounted or stationary. Data are collected along accurately located profiles, usually set-out in a survey grid.

Variable frequency, interchangeable antenna units can be used with the GPR system, depending on the particular application. Low frequency units offer greater depth penetration and are generally better suited for civil engineering and geological site investigations. Small, portable, high frequency units are used for high resolution work involving of concrete and masonry structures.

## 2. Methodology

### 2.1. Electric resistivity technique

The main aim of a resistivity survey is the measurement of the electrical resistivity of the earth, knowledge of which enables the estimation of its hydrogeological properties. The first step toward this is the measurement of the resistance of the ground

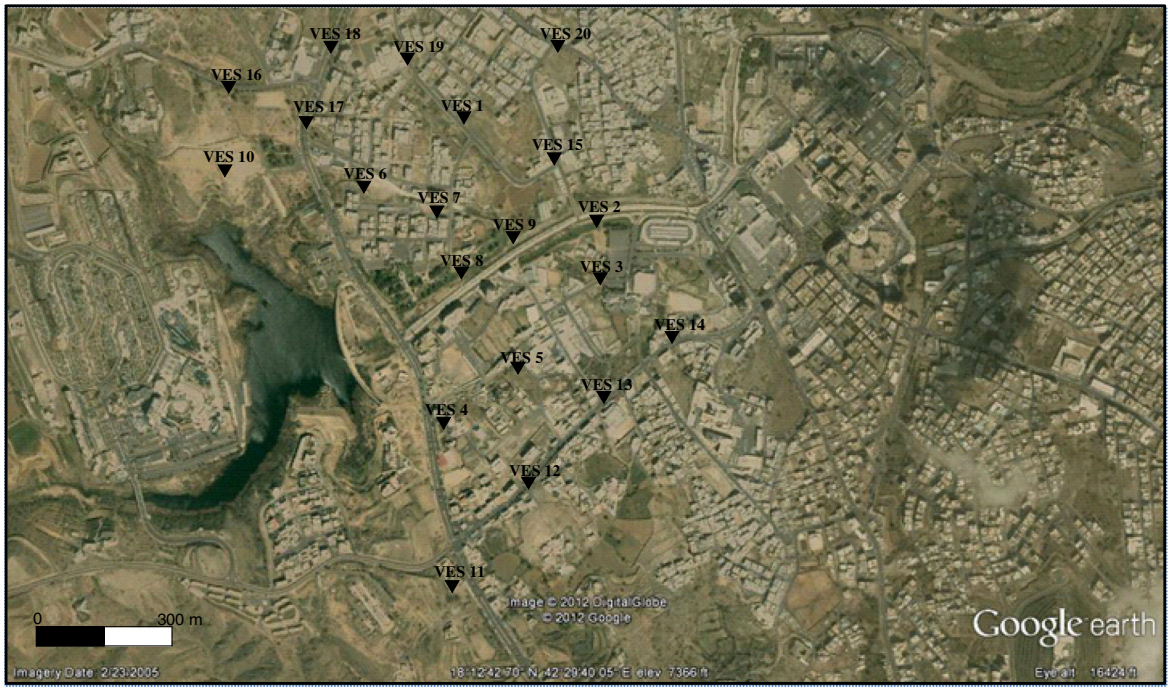


**Fig. 1** Location map VESes around the lake area.

by passing an electrical current into it through metal stakes (electrodes) which acts as the current source. Two short metallic stakes (electrodes) are driven about 1 foot are used to measure the earth voltage (or electrical potential) generated by the current.

### *2.1.1. Field survey*

Twenty vertical electrical sounding (VESs) have been conducted in the area of study using the schlumberger arrangement of current and potential electrodes. Fig. 1 shows the location of VESes (See Table 1).

The electric resistivity of earth was measured at different values of AB/2 and plotted on logarithmic scale to obtain the field data curve, the result of field data curve inversion was done using the IPI2win software to obtain the layered model as shown in Figs. 2–7.

### *2.1.2. Electric data analysis and interpretation*

The interpretation of vertical electrical soundings was conducted using the IPI2win program. Data obtained from these VESes have been used to construct two maps for the depth of water table and the thickness of the water bearing layer as shown in Figs. 8 and 9. Inspection of Fig. 8 shows that, the depth of water bearing layer ranging from 2 m to 10 m, indicates that this area is high structurally controlled. Three main zones were detected; the first one on the front of the dam, the depth has values between 4.5 to about 9 meters. The other two similar zones appear at the edges of the dam, the depth of water bearing layer becomes more less (2–4 m). Then the depth increased to South and North West direction.

Fig. 9 represent the thickness distribution of the water bearing layer, inspection of this figure shows a high thickness at the central part, ranging from 32 m to 44 m, and decreases gradually southward and northward to reach about 10 m.

To obtain the stratigraphic succession in the area of study, a geo-electric cross section has been constructed along the profile containing VESes No. 16, 17, 6, 7, 8, 5 and 12 (Fig. 10). The constructed resistivity geo-electrical cross sections along this profile obtain the presence of three geoelectric layers. The first layer has resistivity values ranging from (44 Ω m–1200 Ω m) with thickness ranging from 3 m to 18 m. This geoelectric layer was interpreted as the wadi deposits.

The second geoelectric layer obtains resistivity values ranging from 11 Ω m–137 Ω m. This geoelectric layer was interpreted as the water saturated fractured basements.

The third geoelectric layer obtain resistivity values ranging from (2200 Ω m–90,000 Ω m) which interpreted as dry, massive basements. Also, this section obtains the presence of two opposite normal faults.

### *2.2. Ground penetrating radar technique*

Ground penetrating radar (GPR) is a high resolution electromagnetic technique that is designed primarily to investigate the shallow subsurface of the earth, building materials, roads and bridges. GPR is a time-dependent geophysical technique that can provide a 3-D pseudo image of the subsurface, including the fourth dimension of color, and can also provide accurate depth estimates for many common subsurface objects. Under favorable conditions, GPR can provide precise information concerning the nature of buried objects. It has also proven to be a tool that can be operated in boreholes to extend the range of investigations away from the boundary of the hole (Bungey, 2004; Benedetto and Pensa, 2007).

In addition to its military and civil applications, GPR is now a very important tool in ground investigations, for near surface to a depth of several tens of meters. It is used for determining the thicknesses of soil horizons and depth to water

**Table 1** Electric resistivity values at different values of AB/2 for each VES.

| AB/2 | MN/2 | V-1 | V2 | V-3 | V-4 | V-5 | V-6 | V-7 | V-8 | V-9 | V-10 |
|---|---|---|---|---|---|---|---|---|---|---|---|
| 3 | 1.2 | 640.2 | 58.5 | 276.6 | 327.9 | 315 | 127.2 | 220.7 | 40.3 | 93.1 | 1369.8 |
| 4 | 1.2 | 675.5 | 59.7 | 238.6 | 227.8 | 218 | 127.5 | 225.2 | 44.4 | 96.1 | 1067.2 |
| 6 | 1.2 | 497.5 | 56.7 | 196.8 | 218 | 215 | 126.9 | 231.2 | 42.3 | 90.8 | 1170.4 |
| 8 | 1.2 | 454.5 | 51.1 | 153 | 173.2 | 169 | 132.8 | 271.2 | 37.7 | 82.4 | 960.8 |
| 10 | 1.2 | 320.4 | 45.4 | 154.5 | 160.5 | 155 | 134.2 | 268.9 | 30.2 | 67.8 | 780.4 |
| 14 | 1.2 | 308.5 | 35.5 | 162.8 | 206 | 205 | 143 | 295.9 | 20.3 | 50.3 | 774 |
| 10 | 4 | 283.3 | 43.8 | 106.3 | 151.6 | 149 | 132.9 | 225.1 | 39.3 | 58.9 | 770 |
| 14 | 4 | 254 | 33.7 | 118.2 | 165.1 | 162 | 138.7 | 248.7 | 24.4 | 42.2 | 773.2 |
| 20 | 4 | 315.2 | 31.9 | 135.1 | 193.1 | 189 | 150.4 | 284.4 | 17.7 | 35.5 | 627.8 |
| 30 | 4 | 508.5 | 31.3 | 163.6 | 178 | 170 | 187.4 | 296.4 | 15 | 31.9 | 481.6 |
| 40 | 4 | 673.7 | 26 | 191.8 | 161.9 | 161.9 | 233.8 | 237.1 | 13.1 | 35.1 | 539.9 |
| 30 | 12 | 398.7 | 31.5 | 160.5 | 150.8 | 149 | 210.4 | 272 | 14.2 | 31.6 | 466.1 |
| 40 | 12 | 556.1 | 26.3 | 189.3 | 173 | 171 | 260.5 | 210.3 | 13.7 | 33.4 | 514.4 |
| 60 | 12 | 795.4 | 23.5 | 245.2 | 202.8 | 201 | 370.8 | 190 | 16.4 | 39 | 613.7 |
| 80 | 12 | 964.5 | 42.6 | 288.3 | 278.4 | 275 | 424.7 | 186.4 | 24.2 | 43 | 519.2 |
| 100 | 12 | 1125.1 | 83.1 | 333.9 | 362.3 | 359 | 560 | 195.8 | 30.4 | 53.7 | 431.1 |
| 140 | 12 | 1500 | 101.2 | 380 | 496.4 | 482 | 713.4 | 219.4 | 52.1 | 72.4 | 396.3 |
| 200 | 12 | | | | | | | | | | 425.4 |
| AB/2 | MN/2 | V-11 | V12 | V-13 | V-14 | V-15 | V-16 | V-17 | V-18 | V-19 | V-20 |
| 3 | 1.2 | 204.4 | 315 | 202 | 198 | 105 | 1450 | 540 | 988 | 631 | 1121 |
| 4 | 1.2 | 223.3 | 218 | 212 | 208 | 88 | 1100 | 530 | 815 | 672 | 982 |
| 6 | 1.2 | 235.2 | 215 | 225 | 230 | 76 | 1170.4 | 421 | 625 | 480 | 870 |
| 8 | 1.2 | 227 | 169 | 227 | 235 | 62 | 980 | 212 | 525 | 450 | 660 |
| 10 | 1.2 | 204.3 | 155 | 200 | 198 | 45.4 | 820 | 134.2 | 456 | 330 | 459 |
| 14 | 1.2 | 167.5 | 205 | 160 | 158 | 35.5 | 774 | 143 | 410 | 310 | 453 |
| 10 | 4 | 206.8 | 149 | 203 | 210 | 42 | 770 | 132.9 | 360 | 272 | 373 |
| 14 | 4 | 169.2 | 162 | 168 | 160 | 33.7 | 771 | 138.7 | 286 | 242 | 242 |
| 20 | 4 | 147.5 | 189 | 140 | 135 | 32 | 620 | 160 | 302 | 302 | 302 |
| 30 | 4 | 182.9 | 170 | 176 | 175 | 31 | 496 | 192 | 498 | 498 | 498 |
| 40 | 4 | 217.3 | 161.9 | 215 | 216 | 35 | 532 | 241 | 660 | 660 | 652 |
| 30 | 12 | 203.3 | 149 | 203.3 | 200 | 46 | 461 | 212 | 510 | 410 | 415 |
| 40 | 12 | 240.9 | 171 | 235 | 242 | 48 | 511 | 271 | 560 | 560 | 715 |
| 60 | 12 | 358.6 | 201 | 345 | 352 | 65 | 621 | 391 | 680 | 740 | 780 |
| 80 | 12 | 473.6 | 275 | 465 | 472 | 82 | 510 | 435 | 780 | 860 | 953 |
| 100 | 12 | 593.4 | 359 | 580 | 591 | 89 | 420 | 571 | 818 | 1113 | 1020 |
| 140 | 12 | 736.2 | 482 | 680 | 670 | 120 | 432 | 715 | 115 | 1430 | 1310 |
| 200 | 12 | | | | | | 521 | | | | |

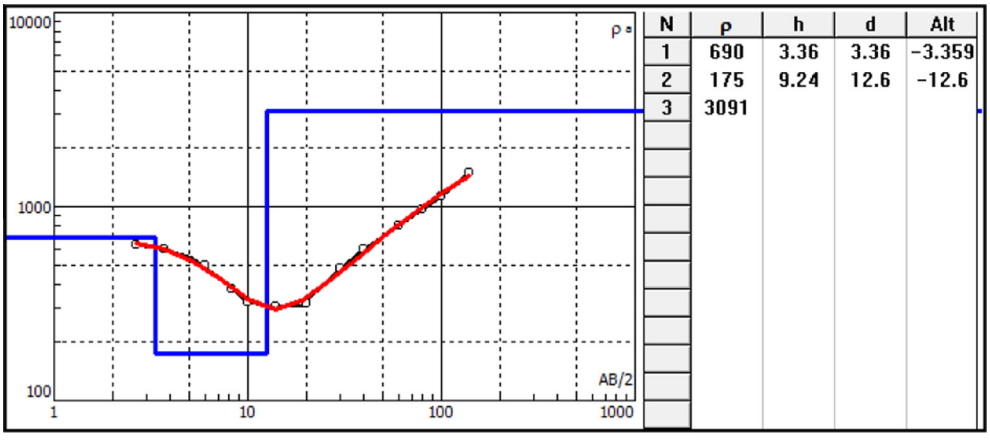


**Fig. 2** The field data and interpreted curve of VES No. 1.

table; detecting air-filled subsurface cavities, buried channels and tunnels, mapping contamination plumes; investigating the condition of dam cores, masonry structures and bridge piers; detecting buried objects in archeological surveys; finding ice or permafrost thicknesses; studying the condition of the asphalt layer on roads, etc (Fruhwirth and Mueller, 1994).

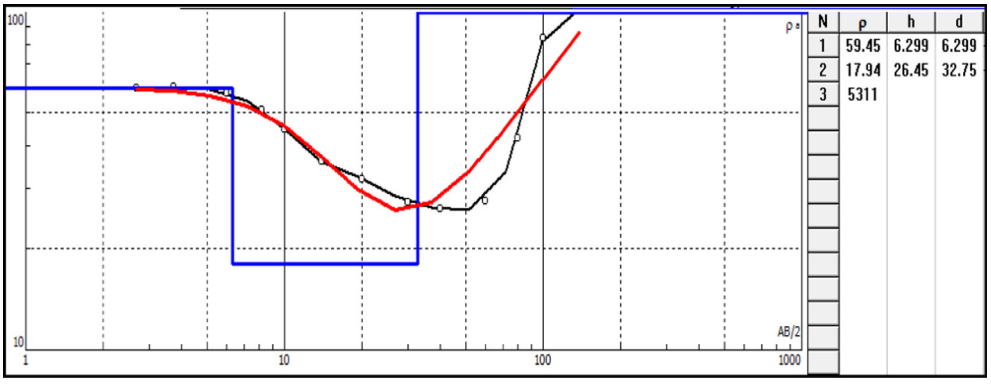


**Fig. 3** The field data and interpreted curve of VES No. 2.

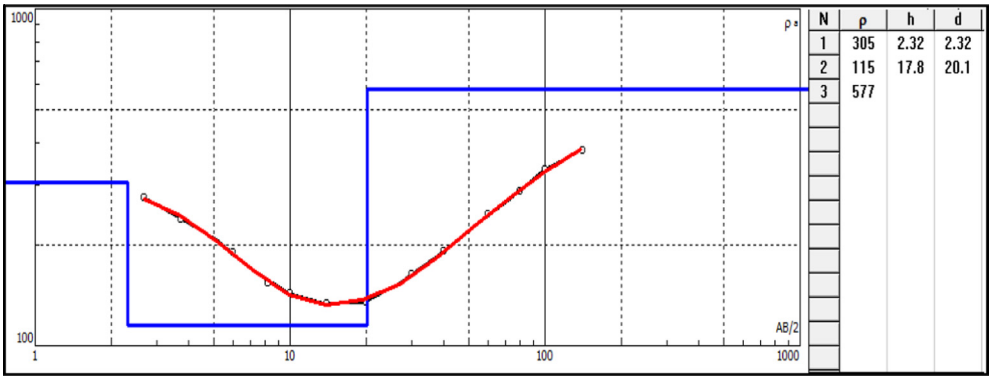


**Fig. 4** The field data and interpreted curve of VES No.3.

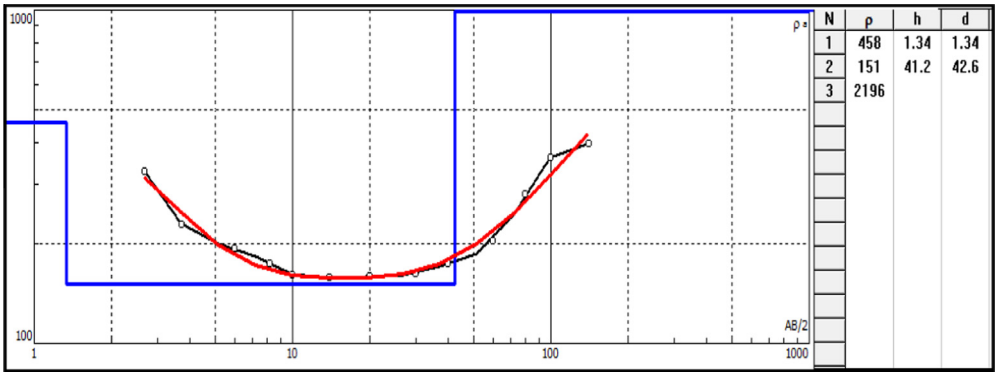


**Fig. 5** The field data and interpreted curve of VES No.4.

*2.2.1. Data acquisition and processing*

A total of 35 GPR profiles were conducted on the body of the dam as shown in Figs. 11 and 12, with different lengths according to the validity of the scanned area. GPR data were acquired using the SIR 3000 system by GSSI equipped with a400 MHz antenna. Data were acquired in continuous mode with a time sampling interval of 512 and a time window of 140 ns.

GPR data were processed using program REFLEX 5.0 to remove the noise signal and to enhance the imbedded features signals. Several processing steps were applied including;

(1) Static correction for the ground zero level,
(2) Background removal to facilitate the recognition of the imbedded infra-structure,
(3) Band-pass 2D filter to remove the noise and get clear sections, and
(4) An automatic gain control (GC).

In the case presented in this paper, the principal objectives of the GPR inspection were:

(1) To detect differences in the reinforced base,
(2) To locate voids and cracks that are not visible on the surface,
(3) To determine the importance of the damage observed on the surface in terms of its depth,
(4) To identify the sections with high moisture content, and

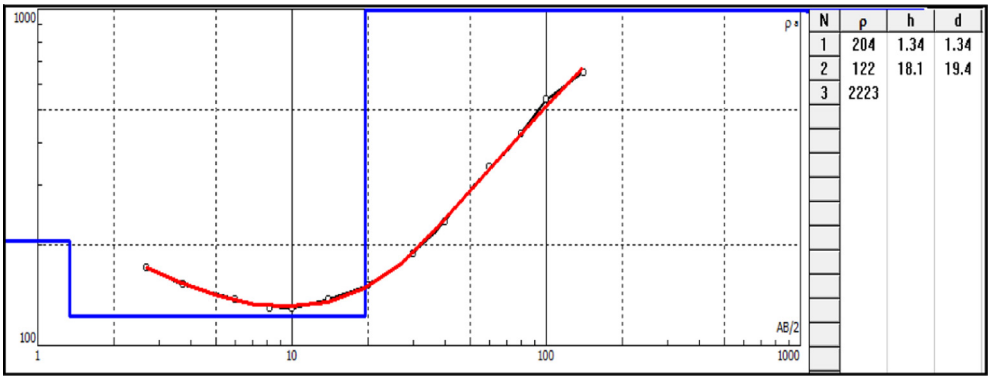


**Fig. 6** The field data and interpreted curve of VES No.6.

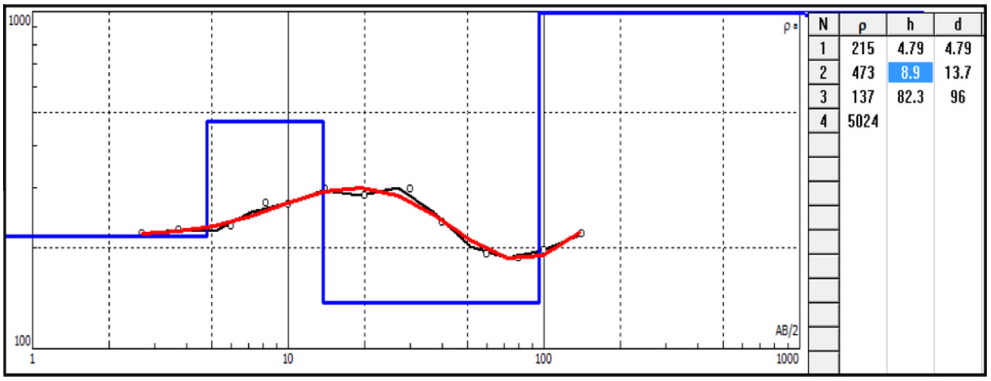


**Fig. 7** The field data and interpreted curve of VES No.7.

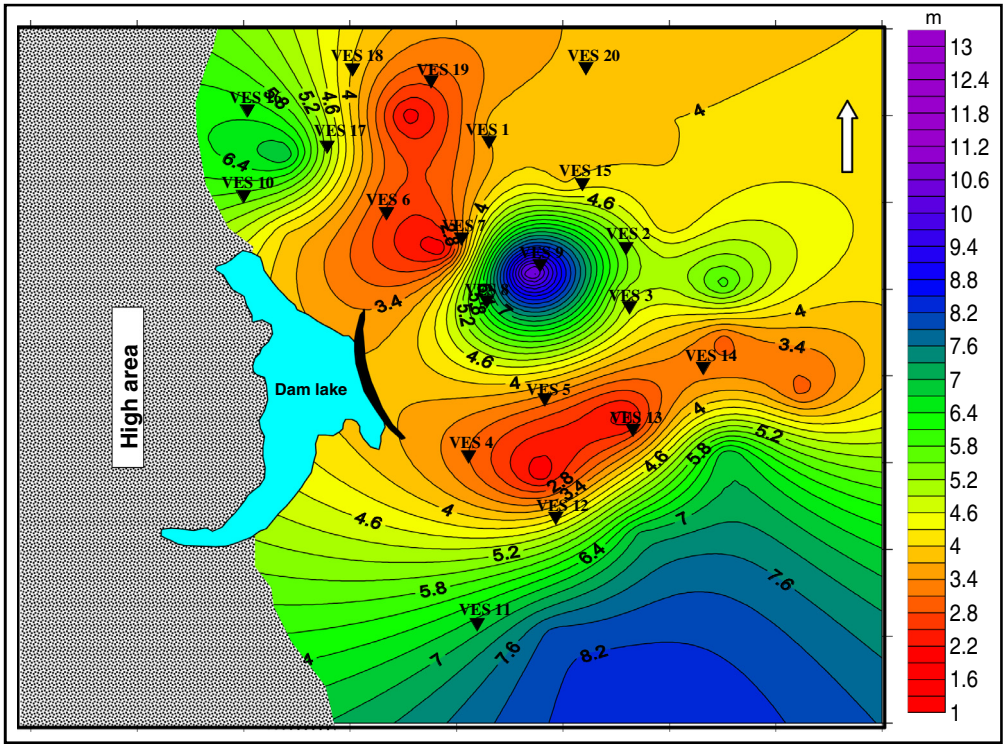


**Fig. 8** Contour map showing the depth to water table as deduced from the VESes analysis.

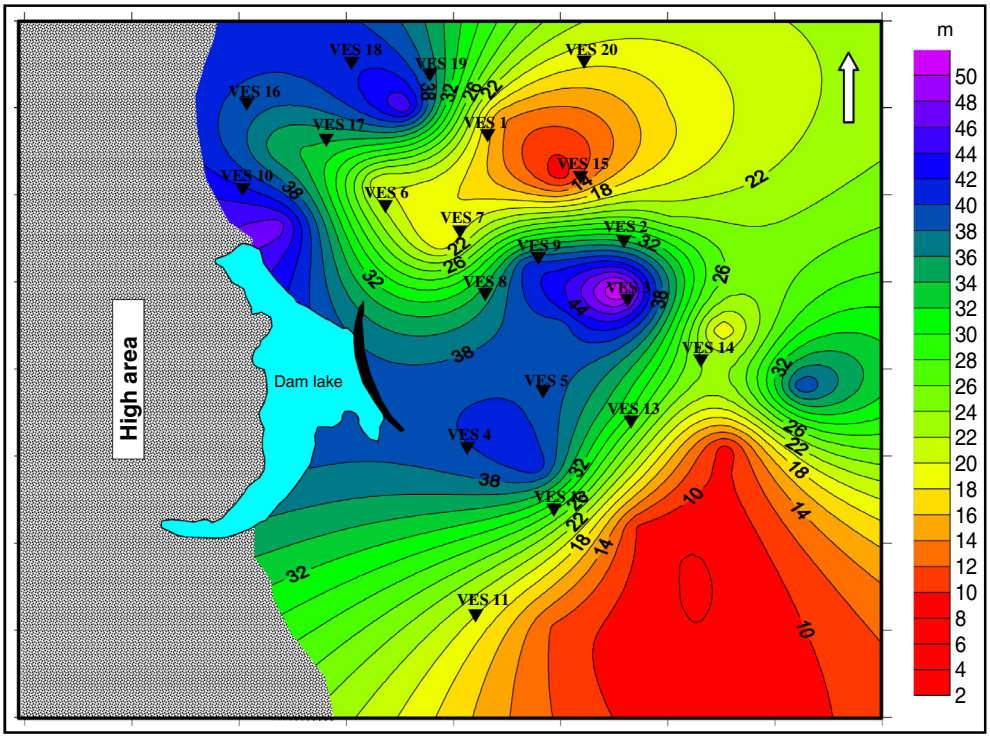


**Fig. 9** Contour map showing the thickness of the water bearing layer as deduced from the VESes analysis.

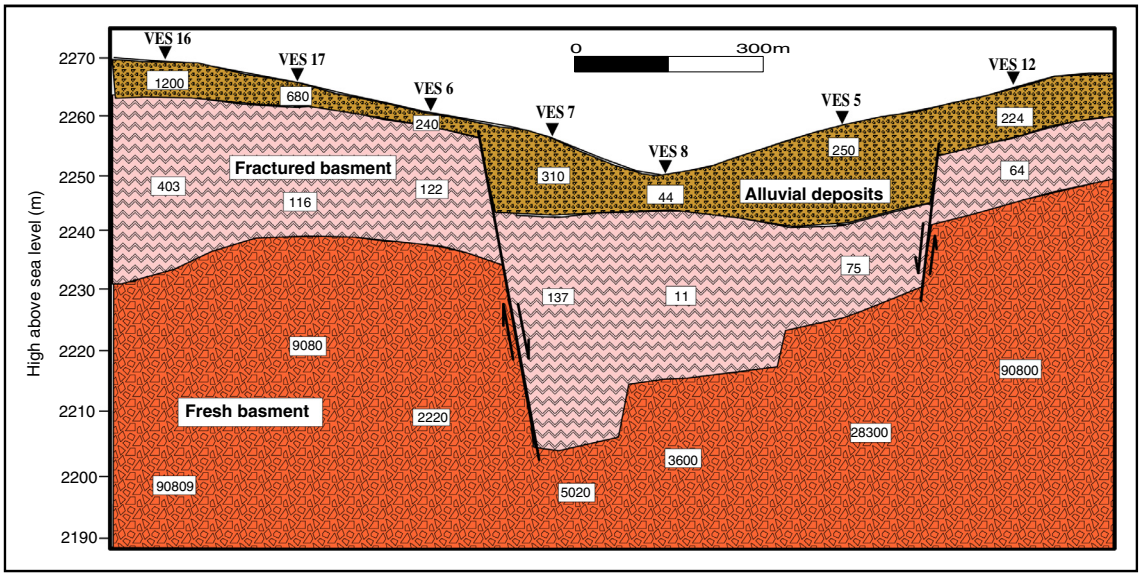


**Fig. 10** A geo-electric cross section constructed along the profile containing VES No. 16, 17, 6, 7, 8, 5 and 12.

(5) To identify the possible causes of the flooding. These data are necessary when deciding on the most effective architectural solutions.

### *2.2.2. GPR data analysis and interpretation*

This case study revolved around the GPR inspection of the reinforced concrete base of the Abha dam. GPR was carried out to determine the existence of any damage, the existence of internal voids or fissures in the slab, changes in the moisture content of the concrete structure. In this study, we were able to determine the probable causes of the differences in the reflected wave propagation recorded times while taking into account the changes in the frequency content and the amplitude of the reflected signal. GPR gives enough resolution to be used in the shallow analysis of civil buildings. It is also useful in locating the probable causes of damage due to damp. The analysis of the radar data frequency content provides valuable information to qualitatively determine the moist zones. The solution to the structural problems was defined using the GPR information and the final maps of the interpreted sections.

The results indicated that GPR analysis could be applied in the study of reinforced concrete slabs and pavement

**Fig. 11** Sketch diagram for the dam body showing the location of the GPR profiles.

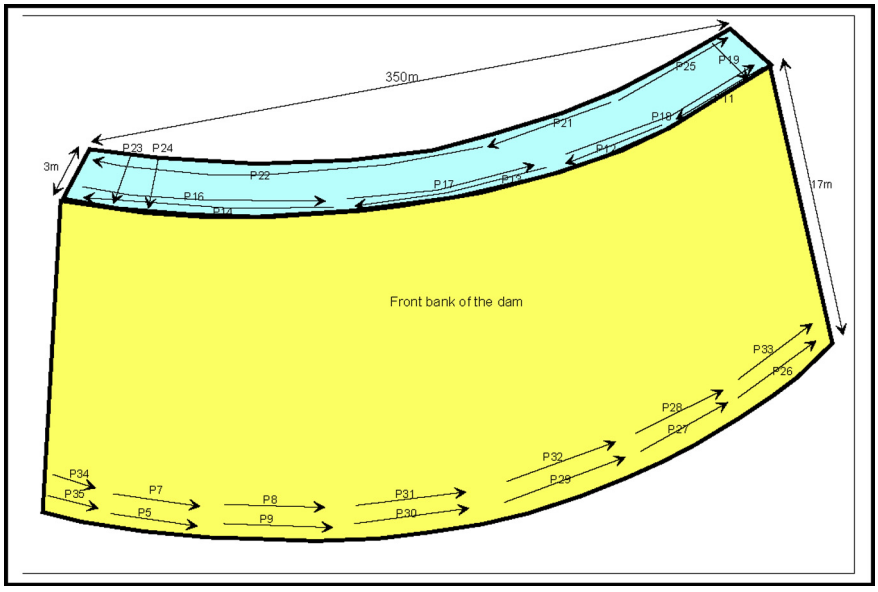


**Fig. 12** Pictures showing the GPR field survey on the front bank and the top of the dam.

diagnostics. Some sections of the GPR profiles conducted on the top of the dam are illustrated in Figs. 13–25, inspections of these records showed that:

The concrete base: The slab is 50 cm thick and its reinforcement is observed in the base. The spatial resolution is enough to detect all the steel bars as different anomalies. We obtained radar images of the areas that showed damage on the surface. The magnitude of the depth of the damage was established in each case. Other interesting anomalies detected were the differences in the two-way travel time of the reflected wave from the bottom of the slab. Two possible explanations were taken into consideration; the variations in the water content and the changes in the slab thickness (Figs. 13–15). The existence of moisture in several zones of the concrete structure: High reflective sections correspond to wetter areas and these zones are related to lower wave velocities. The analysis of these velocities allows the water content in these conflictive zones to be estimated.

The analysis in this study provided internal images of the slab, showing its morphology, areas of possible damage and changes to the structure, and the situation of the steel reinforcements. Estimations of the moisture content in the different areas could also be determined from the GPR data and the information about the structural elements. Despite the necessity of accurate data processing to obtain a precise interpretation of the data, GPR proved to be a fast survey methodology. The joint study of travel times, amplitudes and frequencies seems to be a good way to interpret the GPR data and to select the most accurate interpretation.

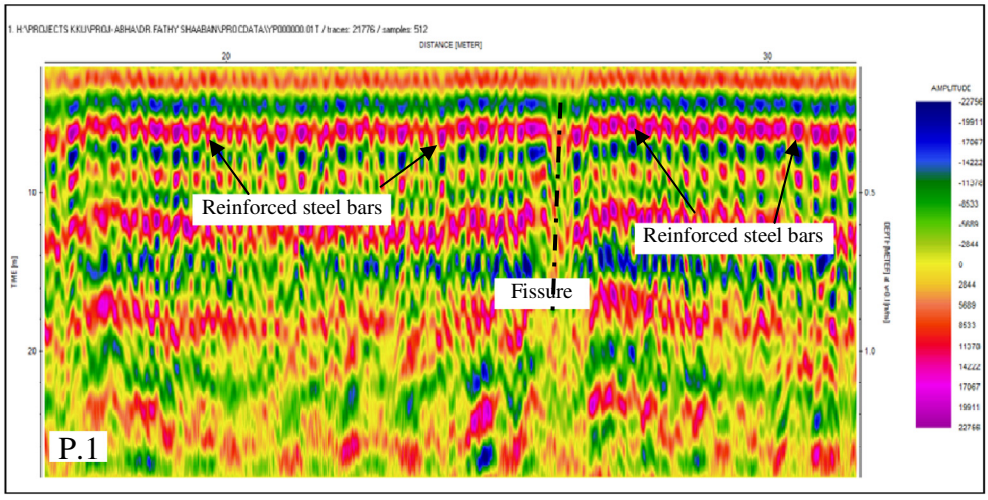


**Fig. 13** A segment of the GPR record No. 12.

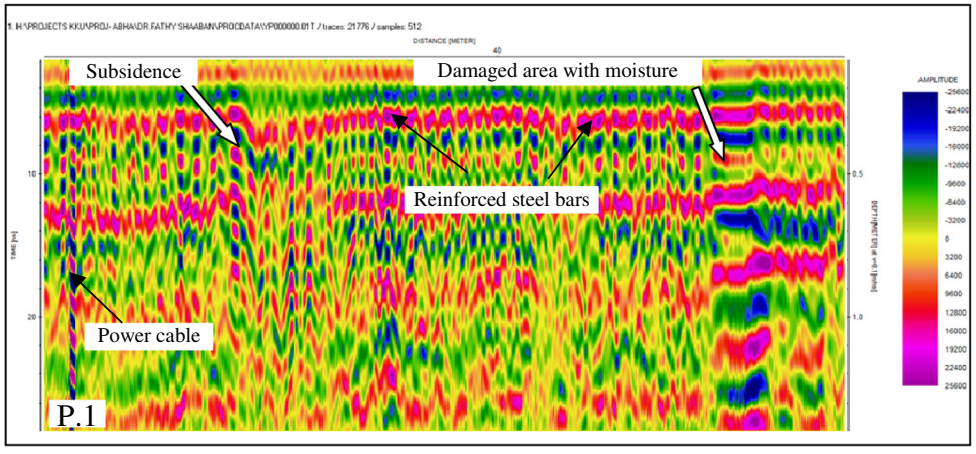


**Fig. 14** A segment of the GPR record No. 12.

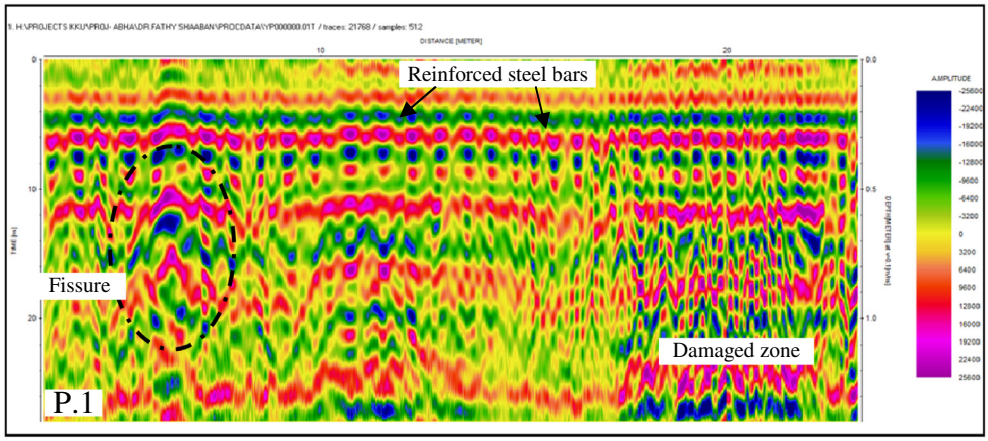


**Fig. 15** A segment of the GPR record No. 13.

The existence of internal cracks in the slabs: The damage was detected through the anomalies recorded in the radar images, and in several profiles these affected zones are closely related to the fissures previously observed on the surface of the slabs. In a few areas the results were checked with specific invasive tests. As the cracks are mainly seen between columns, a

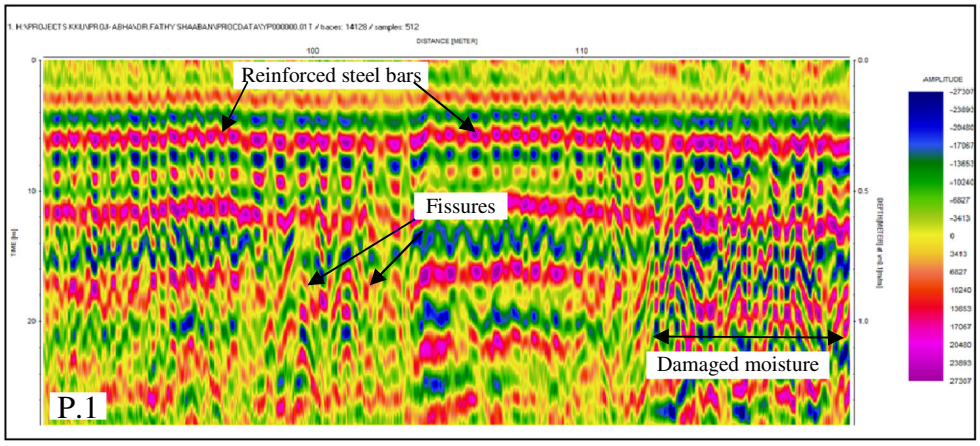


**Fig. 16** A segment of the GPR record No. 14.

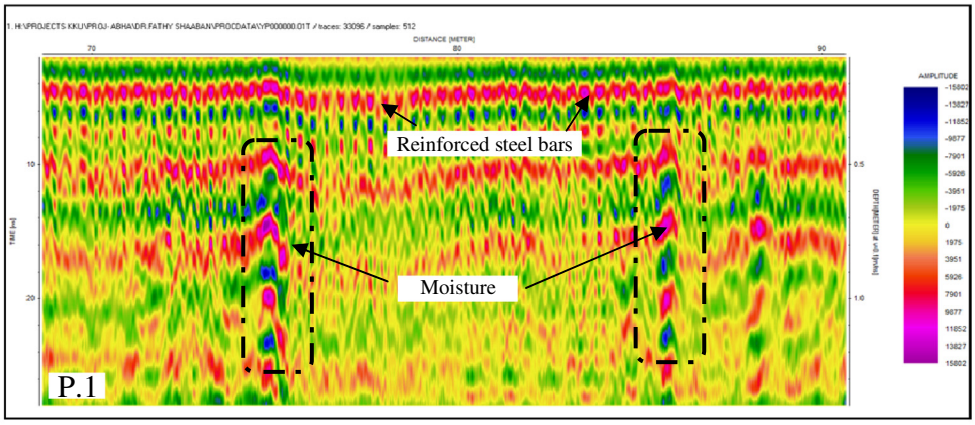


**Fig. 17** A segment of the GPR record No. 18.

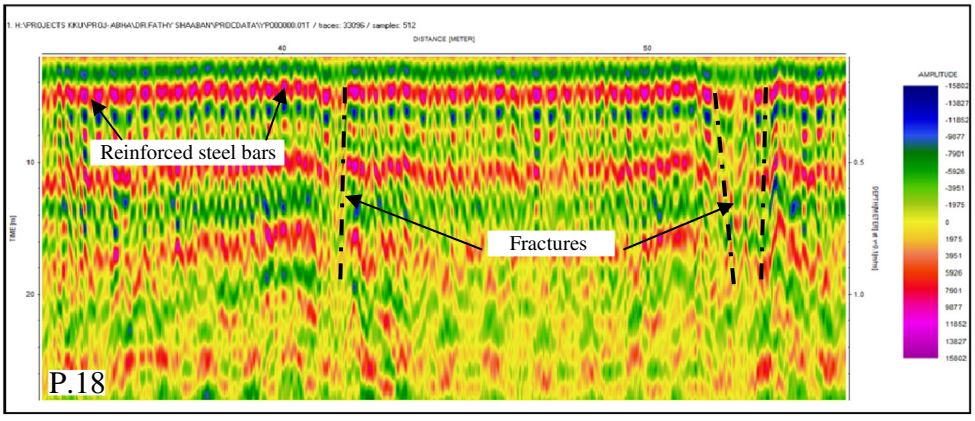


**Fig. 18** A segment of the GPR record No. 18.

possible cause could be the tensile stress produced in these zones (Figs. 16–18).

Figs. 19–22, illustrated other parts of the GPR records conducted on the profiles numbers 21 and 22 at the top of the dam. The position of the steel reinforcement and the possible changes in the slab construction. Data also allowed us to determine the separation of the reinforced bars and the existence of changes in the structure especially in radar record No. 22, Fig. 22.

The GPR section that have been conducted at the foot of the dam, are inspected collectively. Some parts of these images are

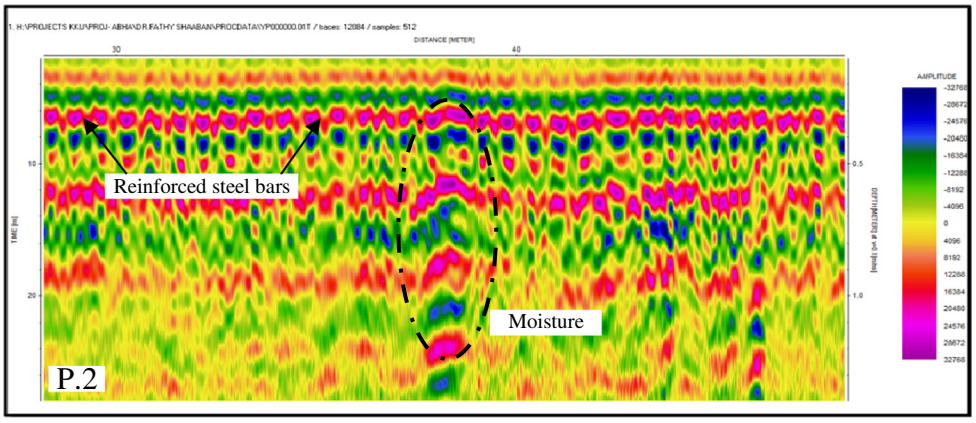


**Fig. 19** A segment of the GPR record No. 21.

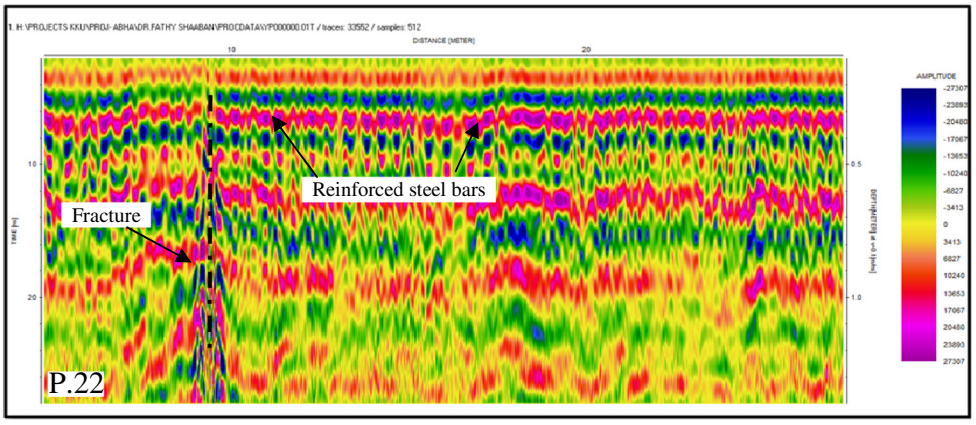


**Fig. 20** A segment of the GPR record No. 22.

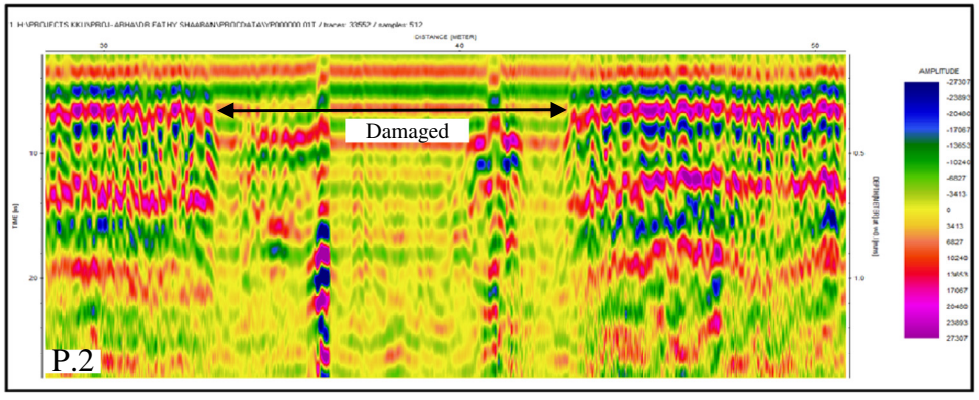


**Fig. 21** A segment of the GPR record No. 22.

illustrated in Figs. 23–25. These images are useful in determining most problematic sections. They also provide information about the zones affected fractures, cavities and high moisture.

## 3. Conclusions

Data obtained from the VESes have been used to construct two maps for the depth for water table and the thickness of the water bearing layer. Both maps indicated that, the depth of water bearing layer ranged from 2 m to 10 m, which means this area is high structurally controlled. Three main zones were detected; the first one on the front of the dam, the depth has values between 4.5 to about 9 meters. The other two similar zones appear at the edges of the dam, the depth of water bearing layer becomes more less (2–4 m).

To obtain the stratigraphic succession in the area of study, a geo-electric cross section has been constructed, showing the

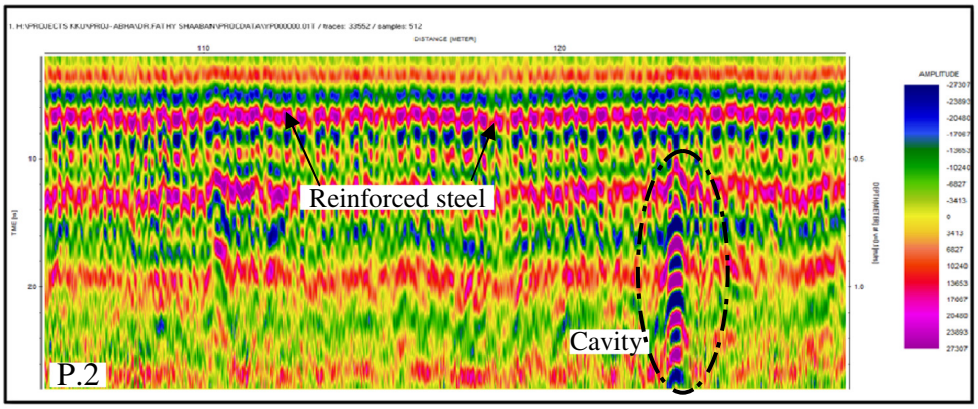


**Fig. 22** A segment of the GPR record No. 22.

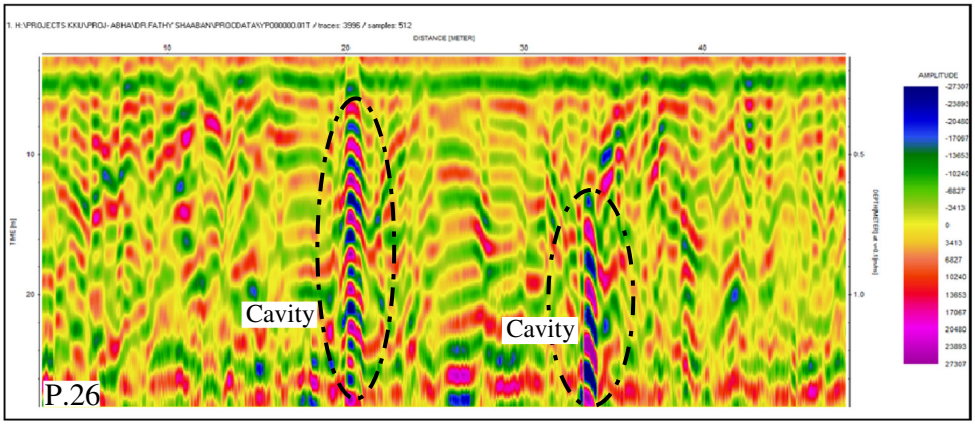


**Fig. 23** A segment of the GPR record No. 26.

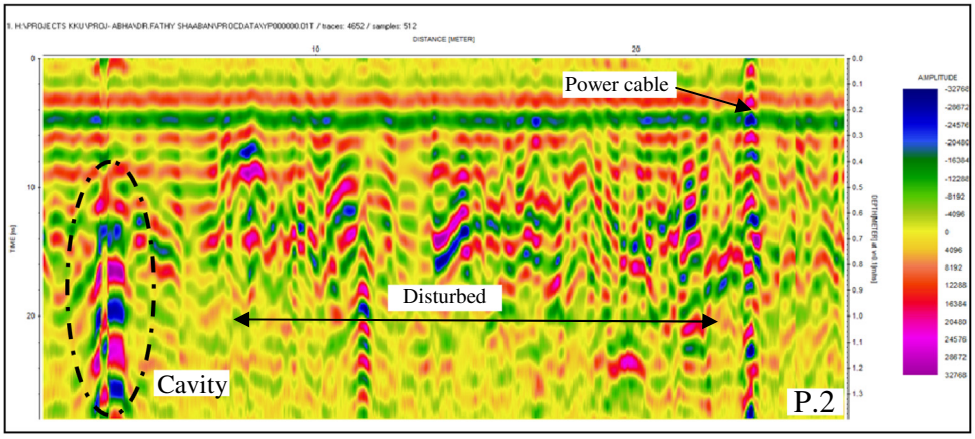


**Fig. 24** A segment of the GPR record No. 27.

presence of three geoelectric layers. The first layer has resistivity values ranging from 44 Ω m–1200 Ω m with thickness ranging from 3 m to 18 m which is interpreted as the wadi deposits. The second geoelectric layer having resistivity values ranging from 11 Ω m–137 Ω m this geoelectric layer was interpreted as the water saturated fractured basements. The third geoelectric layer obtains resistivity values ranging from 2200 Ω m–90,000 Ω m and is interpreted as dry massive basement. Also, two opposite normal faults are noticed in this section.

The analysis of GPR data provided internal images of the slab, showing its morphology, areas of possible damage and changes to the structure, and the situation of the steel

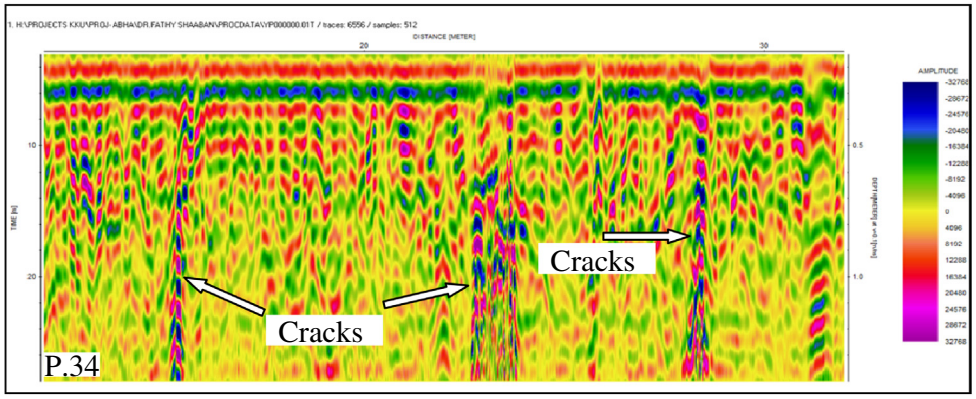


**Fig. 25** A segment of the GPR record No. 34.

reinforcements, the position of the steel reinforcement and the possible changes in the slab construction. Data also allowed us to determine the separation of the reinforced bars and the existence of changes in the structure especially in radar record.

The GPR section that have been conducted at the foot of the dam, are inspected collectively. These images are useful in determining most problematic sections. They also provide information about the zones affected fractures, cavities and high moisture content.

## Acknowledgments

This paper was supported by the scientific research dean at King Khaled University. The author thanks the Dean of Research at the university to assist in the provision of material and technical support required for this search.

## Reference

Andrade, C., Sarria, J., Alonso, C., 1999. Relative humidity in interior of concrete exposed to natural and artificial weathering. Cement Concr. Res. 29, 1249–1259.

Benedetto, A., Pensa, S., 2007. Indirect diagnosis of pavement structural damages using surface GPR reflection techniques. J. Appl. Geophys. 62, 107–123.

Bungey, J.H., 2004. Sub-surface radar testing of concrete: a review. Construct Build Mater. 18, 1–8.

Davis, J.L., Annan, A.P., 1989. Ground penetrating radar for high resolution mapping of soil and rock stratigraphy. Geophys. Prospect. 37 (5), 531–551.

Davis, J.L., Annan, A.P., Vaughan, C.J., 1984. Placer exploration using radar and seismic methods. In: 54th Annual meeting, Soc. Expl. Geophysicist, Expanded Abstracts, pp. 306–308.

Fruhwirth, R., Mueller, R., 1994. Application of ground penetrating radar to geotechnical problems. In: 56th Meeting and Technical Exhibition, European Association of Exploration Geophysicists, Technical Programme and Abstracts of Papers, 56, pp. 1012–1013

Klysz, G., Balayssac, J.-P., Laurens, S., 2004. Spectral analysis of radar surface waves for non-destructive evaluation of cover concrete. NDT & E Int. 37 (3), 221–227.

Laurens, S., 2001. Aptitude de la technique radar à la caractérisation du béton d'enrobage-Aide au diagnostic de la corrosion des armatures. Civil Engineering Doctoral Thesis, INSA de Toulouse (France). University of Sherbrooke, Sherbrooke (Québec, Canada).

Matthews, S., Goodier, A., Massey, S., 1998. Permittivity measurements and analytical dielectric modelling of plain structural concretes. In: Proceedings of the Seventh International Conference on Ground-penetrating Radar, Laurence, Kansas USA, pp. 363–8.

Raupach, M., 1996. Chlorides-induced macrocell corrosion of steel in concrete – theoretical background and practical consequences. Construct Build Mater. 10 (5), 329–338.

Sbartaï, Z.M., 2005. Caractérisation physique des bétons radar – approche neuromimétique de l'inversion. Civil Engineering Doctoral Thesis. Université Paul Sabatier, Toulouse III (France). University of Sherbrooke, Sherbrooke (Québec, Canada).

Sbartaï, Z.M., Laurens, S., Balayssac, J.-P., Arliguie, G., Ballivy, G., 2006a. Ability of the direct wave of radar ground-coupled antenna for NDT of concrete structures. NDT & E Int. 39 (5), 400–407.

Sbartaï, Z.M., Laurens, S., Balayssac, J.-P., Ballivy, G., Arliguie, G., 2006b. Effect of concrete moisture on radar signal amplitude. ACI Mater. 103 (6), 419–426.

Tsoflias, G.P., Van Gestel, J., Stoffa, P.L., Blankenship, D.D., Sen, M.K., 2004. Vertical fracture detection by exploiting the polarization properties of ground-penetrating radar signals. Geophysics 69, 803–810.